arXiv:0910.0593v1 [cond-mat.mes-hall] 4 Oct 2009

Quasi-Ferromagnet Spintronics in Graphene Nanodisk-Lead System

Motohiko Ezawa
Department of Applied Physics, University of Tokyo, Hongo 7-3-1, 113-8656, Japan

A zigzag graphene nanodisk can be interpreted as a quantum dot with an internal degree of freedom. It is well described by the infinite-range Heisenberg model. We have investigated its thermodynamical properties. There exists a quasi-phase transition between the quasi-ferromagnet and quasi-paramagnet states, as signaled by a sharp peak in the specific heat and in the susceptibility. We have also analyzed how thermodynamical properties are affected when two leads are attached to the nanodisk. It is shown that lead effects are described by the many-spin Kondo Hamiltonian. There appears a new peak in the specific heat, and the multiplicity of the ground state becomes just one half of the system without leads. Another lead effect is to enhance the ferromagnetic order. Being a ferromagnet, a nanodisk can be used as a spin filter. Furthermore, since the relaxation time is finite, it is possible to control the spin of the nanodisk by an external spin current. We then propose a rich variety of spintronic devices made of nanodisks and leads, such as spin memory, spin amplifier, spin valve, spin-field-effect transistor, spin diode and spin logic gates such as spin-XNOR gate and spin-XOR gate. Graphene nanodisks could well be basic components of future nanoelectronic and spintronic devices.

I. INTRODUCTION

Graphene nanostructure[1,2,3] has attracted much attention for its potential for future application in nanoelectronics and spintronics. In particular, in graphene nanoribbons[4,5,6,7,8,9,10] the low-energy bands are almost flat at the Fermi level due to the edge states. Such a peculiar band structure has motivated many researchers to investigate their electronic and magnetic properties.

Another basic element of graphene derivatives is a graphene nanodisk[11,12,13,14,15,16,17]. It is a nanometer-scale disk-like material which has a closed edge. There are many type of nanodisks, where typical examples are displayed in Fig.1. Among them, the trigonal zigzag nanodisk is prominent in its electronic and magnetic properties because there exist N-fold degenerated half-filled zero-energy states when its size is N. Furthermore, spins make a strong ferromagnetic order due to the exchange interaction as large as the Coulomb interaction[12], and hence the relaxation time is finite but quite large even if the size N is very small. We have called such a system quasi-ferromagnet[12].

In this paper we make a further study of quasi-ferromagnet by exploring thermodynamical properties of the nanodisk-spin system. The system is well described by the infinite-range Heisenberg model. A nanodisk is interpreted as a quantum dot with an internal degree of freedom. It is exactly solvable. Constructing the partition function, we calculate the specific heat, the entropy, the magnetization and the susceptibility. We find a sharp peak in the specific heat and in the susceptibility, which is interpreted as a quasi-phase transition between the quasi-ferromagnet and quasi-paramagnet states.

We then investigate a nanodisk-lead system, where the lead is made of a zigzag graphene nanoribbon or an ordinary metallic wire. (We refer to it as a graphene lead or a metallic lead for brevity.) We perform the Schrieffer-Wolff transformation to derive the many-spin Kondo Hamiltonian describing the lead effects. Constructing the partition function, we analyze thermodynamical properties. There appears a new peak in the specific heat but not in the susceptibility for small size nanodisks, $N \lesssim 10$. Near the peak the internal energy is found to decrease. We show in the instance of the metallic lead that the band width of free electrons in the lead becomes narrower due to the Kondo coupling. We interpret this phenomenon to mean that some free electrons in the lead are consumed to make spin coupling with electrons in the nanodisk. Furthermore, the multiplicity of the ground state becomes just one half of that in the system without leads. They are indications of Kondo effects due to the Kondo interaction between electrons in the lead and the nanodisk.

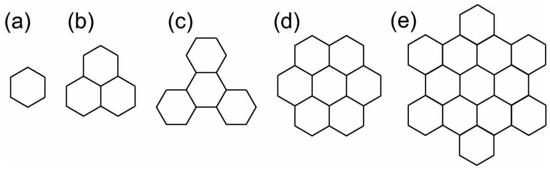

FIG. 1: Basic configurations of typical graphene nanodisks. (a) Benzene. (b) Trigonal zigzag nanodisk (phenalene). (c) Trigonal armchair nanodisk (triphenylene). (d) Hexagonal zigzag nanodisk (coronene). (e) Hexagonal armchair nanodisk (hexa benzocoronene)[18].

With respect to the ferromagnetic order, we find that the lead effect is to enhance the order. This is an important property to fabricate spintronic circuits by connecting leads to nanodisks in nanodevices. Being a ferromagnet, a nanodisk can be used as a spin filter. Furthermore, since the relaxation time is finite, it is possible to control the spin of the nanodisk by an external spin current. We propose a rich variety of spintronic devices made of nanodisks and leads, such as spin memory, spin amplifier, spin valve, spin-field-effect transistor, spin diode and spin logic gates such as spin-XNOR gate and spin-XOR gate. Graphene nanodisks could well be basic components of

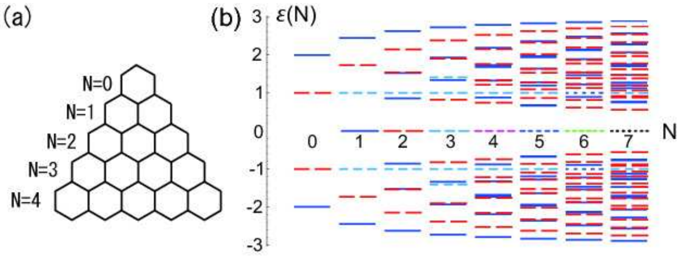

FIG. 2: (a) Geometric configuration of trigonal zigzag nanodisks. It is convenient to introduce the size parameter N in this way. The 0-trigonal nanodisk consists of a single Benzene, and so on. The number of carbon atoms are related as $N_{\mathrm{C}} = N^2 + 6N + 6$. (b) Density of states of the N-trigonal nanodisk for $N = 0, 1, 2, \cdots, 7$. The horizontal axis is the size N and the vertical axis is the energy $\varepsilon(N)$ in units of $t = 2.7$eV. Dots on colored bar indicate the degeneracy of energy levels.

future nanoelectronic and spintronic devices.

This paper is organized as follows. In Sec.II, we summarize the basic notion of trigonal zigzag nanodisks. The low-energy physics is described by electrons in the N-fold degenerated zero-energy sector, which form a quasi-ferromagnet due to large exchange interactions. We also analyze thermodynamical properties of the nanodisk-spin system. In Sec.III, we derive the many-spin Kondo Hamiltonian by the Schrieffer-Wolff transformation in the nanodisk-spin system coupled with graphene leads and also metallic leads. The partition function is calculated in the two steps. First, we perform a functional integration over the lead-electron degree of freedom. Second, we sum up over the nanodisk-spin degree of freedom. We then analyze thermodynamical properties of the nanodisk-lead system. In Sec.IV, we propose some spintronics devices made of nanodisks and leads.

II. NANODISK QUASI-FERROMAGNETS

A. Zero-Energy Sector

We calculate the energy spectra of graphene derivatives based on the nearest-neighbor tight-binding model, which has been successfully applied to the studies of carbon nanotubes and nanoribbons. The Hamiltonian is defined by

$$H = \sum_i \varepsilon_i c_i^\dagger c_i + \sum_{\langle i,j\rangle} t_{ij} c_i^\dagger c_j, \tag{2.1}$$

where ε_i is the site energy, t_{ij} is the transfer energy, and $c_i^\dagger$ is the creation operator of the π electron at the site i. The summation is taken over all nearest neighboring sites $\langle i,j\rangle$. Owing to their homogeneous geometrical configuration, we may take constant values for these energies, $\varepsilon_i = \varepsilon_{\mathrm{F}}$ and $t_{ij} = t \approx 2.70$eV. Then, the diagonal term in (2.1) yields just a constant, $\varepsilon_{\mathrm{F}} N_{\mathrm{C}}$, where N_{C} is the number of carbon atoms in the system. The Hamiltonian (2.1) yields the Dirac electrons for graphene[1,2,3]. There exists one electron per one carbon and the band-filling factor is $1/2$. It is customary to choose the zero-energy level of the tight-binding Hamiltonian (2.1) at this point so that the energy spectrum is symmetric between the positive and negative energy states. Therefore, the system is metallic provided that there exists zero-energy states in the spectrum. A comment is in order. It is understood that carbon atoms at edges are terminated by hydrogen atoms. We carry out the calculation[5,12] together with this condition.

It is straightforward to derive the energy spectrum E_i together with its degeneracy g_i for each nanodisk by diagonalizing the Hamiltonian (2.1). The density of state is given by

$$D(\varepsilon) = \sum_{i=1}^{N_{\mathrm{C}}} g_i \delta(\varepsilon - E_i). \tag{2.2}$$

We have found that the emergence of zero-energy states is surprisingly rare. Among typical nanodisks, only trigonal zigzag nanodisks have degenerate zero-energy states and show metallic ferromagnetism. As an example we display the density of state (2.2) of trigonal zigzag nanodisks in Fig.2. We have classified them by the size parameter N as defined in Fig.2(a), in terms of which the number of carbons is given by $N_{\mathrm{C}} = N^2 + 6N + 6$.

The size-N nanodisk has N-fold degenerated zero-energy states, where the gap energy is as large as a few eV. Hence it is a good approximation to investigate the electron-electron interaction physics only in the zero-energy sector, by projecting the system to the subspace made of those zero-energy states. The zero-energy sector consists of N orthonormal states $|f_\alpha\rangle$, $\alpha = 1, 2, \cdots, N$, together with the SU(N) symmetry. We can expand the wave function of the state $|f_\alpha\rangle$ as

$$f_\alpha(\boldsymbol{x}) = \sum_i \omega_i^\alpha \varphi_i(\boldsymbol{x}), \tag{2.3}$$

where $\varphi_i(\boldsymbol{x})$ is the Wannier function localized at the site i. The amplitude ω_i^α is calculable by diagonalizing the Hamiltonian (2.1). All of them are found to be real. It is intriguing that one of the wave functions is entirely localized on edge sites for the nanodisk with N =odd, as in Fig.3, where the solid (open) circles denote the amplitude ω_i are positive (negative). The amplitude is proportional to the radius of circle. Such a wave function does not exist for the nanodisk with N =even.

B. Coulomb Interactions

We include the Coulomb interaction between electrons in the zero-energy sector[15]. It is straightforward to rewrite the Coulomb Hamiltonian as $H_{\mathrm{D}} = H_{\mathrm{S}} + H_{\mathrm{U}}$

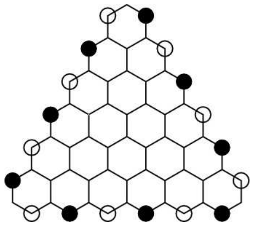

FIG. 3: The zero-energy states of the trigonal nanodisk with size $N = 5$. There are 5 degenerate states. The solid (open) circles denote the amplitude ω_i are positive (negative). The amplitude is proportional to the radius of circle. Electrons are entirely localized on edges in one of the states.

with

$$H_{\rm S} = -2\sum_{\alpha>\beta} J_{\alpha\beta}\boldsymbol{S}(\alpha)\cdot\boldsymbol{S}(\beta), \tag{2.4a}$$

$$H_{\rm U} = \sum_{\alpha>\beta}\left(U_{\alpha\beta} - \frac{1}{2}J_{\alpha\beta}\right) n(\alpha)\, n(\beta) + \sum_{\alpha} U_{\alpha\alpha} n(\alpha), \tag{2.4b}$$

where $U_{\alpha\beta}$ and $J_{\alpha\beta}$ are the Coulomb energy and the exchange energy between electrons in the states $|f_\alpha\rangle$ and $|f_\beta\rangle$. Here, $n(\alpha)$ is the number operator and $\boldsymbol{S}(\alpha)$ is the spin operator,

$$n(\alpha) = \sum_\sigma d_\sigma^\dagger(\alpha) d_\sigma(\alpha), \tag{2.5a}$$

$$\boldsymbol{S}(\alpha) = \frac{1}{2}\sum_{\sigma\sigma'} d_\sigma^\dagger(\alpha)\boldsymbol{\tau}_{\sigma\sigma'} d_{\sigma'}(\alpha), \tag{2.5b}$$

with $d_\sigma(\alpha)$ the annihilation operator of electron with spin $\sigma = \uparrow, \downarrow$ in the state $|f_\alpha\rangle$; $\boldsymbol{\tau}$ is the Pauli matrix.

The remarkable feature is that there exists a large overlap between the wave functions $f_\alpha(\boldsymbol{x})$ and $f_\beta(\boldsymbol{x})$, $\alpha \neq \beta$, since the state $|f_\alpha\rangle$ is an ensemble of sites as in (2.3) and identical sites are included in $|f_\alpha\rangle$ and $|f_\beta\rangle$. Consequently, the dominant contributions come from the on-site Coulomb terms not only for the Coulomb energy but also for the exchange energy. Indeed, it follows that $U_{\alpha\beta} = J_{\alpha\beta}$ in the on-site approximation. We thus obtain

$$U_{\alpha\beta} \simeq J_{\alpha\beta} \simeq U\sum_i (\omega_i^\alpha \omega_i^\beta)^2, \tag{2.6}$$

where

$$U \equiv \int d^3x d^3y\ \varphi_i^*(\boldsymbol{x})\varphi_i(\boldsymbol{x}) V(\boldsymbol{x}-\boldsymbol{y})\varphi_i^*(\boldsymbol{y})\varphi_i(\boldsymbol{y}), \tag{2.7}$$

with the Coulomb potential $V(\boldsymbol{x}-\boldsymbol{y})$. The Coulomb energy U is of the order of 1eV because the lattice spacing of the carbon atoms is ~ 1Å in graphene. Coulomb blockade peaks appear at $\mu = \varepsilon_\alpha$ and $\mu = \varepsilon_\alpha + U_{\alpha\beta}$, where new channels open[15]. We can determine experimentally the energy ε_α and $U_{\alpha\beta}$ by identifying Coulomb blockade peaks.

C. SU(N) Approximation

Since the exchange energy $J_{\alpha\beta}$ is as large as the Coulomb energy $U_{\alpha\beta}$, the spin stiffness $J_{\alpha\beta}$ is quite large. Furthermore, we have checked[15] numerically that all $J_{\alpha\beta}$ are of the same order of magnitude for any pair of α and β, implying that the SU(N) symmetry is broken but not so strongly in the Hamiltonian (2.4a). It is a good approximation to start with the exact SU(N) symmetry. Then, the zero-energy sector is described by the Hamiltonian $H_{\rm D} = H_{\rm S} + H_{\rm U}$, with

$$H_{\rm S} = -J\sum_{\alpha\neq\beta}\boldsymbol{S}(\alpha)\cdot\boldsymbol{S}(\beta), \tag{2.8a}$$

$$H_{\rm U} = \left(\frac{U}{2} - \frac{J}{4}\right)\sum_{\alpha\neq\beta} n(\alpha)\, n(\beta) + U\sum_\alpha n(\alpha), \tag{2.8b}$$

where $J \approx U$. The term $H_{\rm S}$ is known as the infinite-range Heisenberg model. We rewrite them as

$$H_{\rm S} = -J\boldsymbol{S}_{\rm tot}^2 + \frac{3}{4}Jn_{\rm tot}, \tag{2.9a}$$

$$H_{\rm U} = \left(\frac{U}{2} - \frac{J}{4}\right)(n_{\rm tot}^2 + 1), \tag{2.9b}$$

where $\boldsymbol{S}_{\rm tot} = \sum_\alpha \boldsymbol{S}(\alpha)$ is the total spin, and $n_{\rm tot} = \sum_\alpha n(\alpha)$ is the total electron number.

The ground states of nanodisks are half filled. We restrict the Hilbert space to the half-filling sector,

$$n(\alpha) = n_\uparrow(\alpha) + n_\downarrow(\alpha) = 1. \tag{2.10}$$

The Hamiltonian (2.9a) is reduced to the Heisenberg model,

$$H_{\rm S} = -J\boldsymbol{S}_{\rm tot}\cdot\boldsymbol{S}_{\rm tot}, \tag{2.11}$$

where we have neglected an irrelevant constant term, $(3/4)JN$. This is exactly diagonalizable, $H_{\rm S}|\Psi\rangle = E_s|\Psi\rangle$, with

$$E_s = -Js(s+1), \tag{2.12}$$

where s takes values from $N/2$ down to $1/2$ or 0, depending on whether N is odd or even,

$$s = \frac{N}{2}, \frac{N}{2} - 1, \frac{N}{2} - 2, \cdots, \qquad s \geq 0. \tag{2.13}$$

The Hilbert space is diagonalized,

$$\mathbb{H} = \otimes^N \mathbb{H}_{1/2} = \oplus^{g_N(s)}\mathbb{H}_s, \tag{2.14}$$

where $\mathcal{H}_s$ denotes the $(2s+1)$ dimensional Hilbert space associate with an irreducible representation of SU(2). The multiplicities $g_N(s)$ satisfies the recursion relation coming from the spin synthesizing rule,

$$g_N(s) = g_{N-1}\left(s - \frac{1}{2}\right) + g_{N-1}\left(s + \frac{1}{2}\right). \tag{2.15}$$

We solve this as

$$g_N\left(\frac{N}{2}-q\right) = {}_N C_q - {}_N C_{q-1}. \tag{2.16}$$

The total degeneracy of the energy level E_s is $(2s+1)\, g_N(s)$.

At half filling, the eigenstate of the Hamiltonian $H_{\rm D}$ is labeled as $|\Psi\rangle = |n_{\rm tot}, s, m\rangle$, where s is the total spin and m is its z-component. We refer to the total spin $\boldsymbol{S}_{\rm tot}$ of a nanodisk as the nanodisk spin.

D. Thermodynamical Properties

We have a complete set of the eigenenergies together with their degeneracies. The partition function of the nanodisk with size N is exactly calculable,

$$\begin{aligned} Z_{\rm S} &= \sum_s (2s+1)\, g_N(s) e^{-\beta E_s} \\ &= \sum_{q=0}^{N/2} (N-2q+1)\left({}_N C_q - {}_N C_{q-1}\right) \\ &\times \exp\left[\beta J\left(\frac{N}{2}-q\right)\left(\frac{N}{2}-q+1\right)\right]. \end{aligned} \tag{2.17}$$

According to the standard procedure we can evaluate the specific heat $C(T)$, the entropy $S(T)$, the magnetization $\langle \boldsymbol{S}_{\rm tot}^2 \rangle$ and the susceptibility $\chi = \frac{1}{k_{\rm B}T}\left(\langle \boldsymbol{S}_{\rm tot}^2\rangle - \langle \boldsymbol{S}_{\rm tot}\rangle^2\right)$ from this partition function, where

$$S_g = \sqrt{\frac{N}{2}\left(\frac{N}{2}+1\right)} \tag{2.18}$$

is the ground-state value of the total spin. The entropy is given by

$$S(0) = k_{\rm B} \log(N+1) \tag{2.19}$$

at zero temperature. We display them in Fig.4 for size $N = 1, 2, 2^2, \cdots 2^{10}$.

There appear singularities in thermodynamical quantities as $N \to \infty$, which represent a phase transition at T_c between the ferromagnet and paramagnet states,

$$T_c = \frac{JN}{2k_{\rm B}}. \tag{2.20}$$

For finite N, there are steep changes around T_c, though they are not singularities. It is not a phase transition. However, it would be reasonable to call it a quasi-phase transition between the quasi-ferromagnet and quasi-paramagnet states. Such a quasi-phase transition is manifest even in finite systems with $N = 100 \sim 1000$.

The specific heat and the magnetization take nonzero-values for $T > T_c$ [Fig.4(a),(c)], which is zero in the limit $N \to \infty$. The entropy for $T > T_c$ is lower than that of the paramagnet [Fig.4(b)]. These results indicate the existence of some correlations in the quasi-paramagnet state. The maximum value of the susceptibility increases linearly as N becomes large. It is an indicator of the quasi-phase transition.

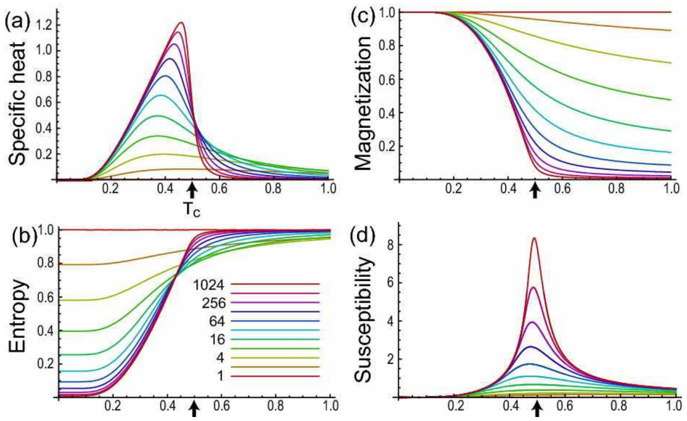

FIG. 4: Thermodynamical properties of the nanodisk-spin system. (a) The specific heat C in unit of $k_{\rm B}N$. (b) The entropy S in unit of $k_{\rm B}N \log 2$. (c) The magnetization $\langle \boldsymbol{S}_{\rm tot}^2 \rangle$ in unit of S_g^2. (d) The susceptibility χ in unit of S_g. The size is $N = 1, 2, 2^2, \cdots 2^{10}$. The horizontal axis stands for the temperature T in unit of $JN/k_{\rm B}$. The arrow represents the phase transition point T_c in the limit $N \to \infty$.

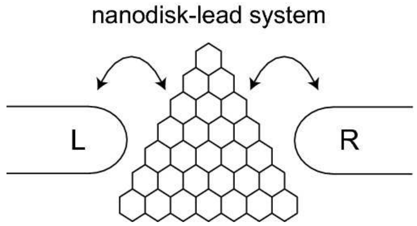

FIG. 5: The nanodisk-lead system. The nanodisk with $N = 7$ is connected to the right and left leads by tunneling coupling $t_{\rm R}$ and $t_{\rm L}$.

III. MANY-SPIN KONDO EFFECTS

We proceed to investigate how thermodynamical properties of the nanodisk is affected by the attachment of the leads. The nanodisk is no longer in the half-filled state, when charges transfer between the nanodisk and the leads. However, the nanodisk remains to be half filled, when a charge transfers from the lead to the nanodisk and then transfers back from the nanodisk to the lead. Such a process is the second order effect in the tunneling coupling constant $\tilde{t}$. We now show that it is described by the many-spin Kondo Hamiltonian.

A. Nanodisk-Lead System

We analyze a system made of a nanodisk connected to two leads [Fig.5]. The model Hamiltonian is given by

$$H=H_{\mathrm{S}}+H_{\mathrm{U}}+H_{\mathrm{L}}+H_{\mathrm{TL}}+H_{\mathrm{TR}}. \tag{3.1}$$

Here, H_{L} is the lead Hamiltonian,

$$H_{\mathrm{L}}=\sum_{k\sigma}\varepsilon\left(k\right)(c_{k\sigma}^{\mathrm{L}\dagger}c_{k\sigma}^{\mathrm{L}}+c_{k\sigma}^{\mathrm{R}\dagger}c_{k\sigma}^{\mathrm{R}}), \tag{3.2}$$

describing a noninteracting electron gas in the leads with the dispersion relation $\varepsilon\left(k\right)$, where $c_{k\sigma}^{\chi}$ is the annihilation operator of electron with the wave number k and the spin σ in the left (χ =L) or right (χ =R) lead. On the other hand, H_{TL} and H_{TR} are the transfer Hamiltonians between the left (L) and right (R) leads and the nanodisk, respectively,

$$H_{\mathrm{TL}}=t_{\mathrm{L}}\sum_{k\sigma}\sum_{\alpha}[c_{k\sigma}^{\mathrm{L}\dagger}d_{\sigma}(\alpha)+d_{\sigma}^{\dagger}(\alpha)c_{k\sigma}^{\mathrm{L}}], \tag{3.3a}$$

$$H_{\mathrm{TR}}=t_{\mathrm{R}}\sum_{k\sigma}\sum_{\alpha}[c_{k\sigma}^{\mathrm{R}\dagger}d_{\sigma}(\alpha)+d_{\sigma}^{\dagger}(\alpha)c_{k\sigma}^{\mathrm{R}}], \tag{3.3b}$$

with t_{χ} the tunneling coupling constant. We have assumed that the spin does not flip in the tunneling process.

The nanodisk-lead system looks similar to that of the N-dot system.[19] However, there exists a crucial difference. On one hand, in the ordinary N-dot system, an electron hops from one dot to another dot. On the other hand, in our nanodisk system, the index α of the Hamiltonian runs over the N-fold degenerate states and not over the sites. According to the Hamiltonian (3.3), an electron does not hop from one state to another state. Hence, it is more appropriate to regard our nanodisk as a one-dot system with an internal degree of freedom.

It is convenient to make the transformation

$$\begin{pmatrix} c_{k\sigma}^{\mathrm{e}} \\ c_{k\sigma}^{\mathrm{o}} \end{pmatrix}=\frac{1}{\tilde{t}}\begin{pmatrix} t_{\mathrm{L}}^{*} & t_{\mathrm{R}}^{*} \\ -t_{\mathrm{R}} & t_{\mathrm{L}} \end{pmatrix}\begin{pmatrix} c_{k\sigma}^{\mathrm{L}} \\ c_{k\sigma}^{\mathrm{R}} \end{pmatrix} \tag{3.4}$$

with

$$\tilde{t}=\sqrt{\left|t_{L}\right|^{2}+\left|t_{R}\right|^{2}}, \tag{3.5}$$

so that the right and left leads are combined into the "even" and "odd" leads. The lead Hamiltonian H_{L} is invariant under above transformation,

$$H_{\mathrm{L}}=\sum_{k\sigma}\varepsilon\left(k\right)\left(c_{k\sigma}^{\mathrm{e}\dagger}c_{k\sigma}^{\mathrm{e}}+c_{k\sigma}^{\mathrm{o}\dagger}c_{k\sigma}^{\mathrm{o}}\right), \tag{3.6}$$

but the transfer Hamiltonian is considerably simplified,

$$H_{\mathrm{T}}=\tilde{t}\sum_{k\sigma}\sum_{\alpha}\left(c_{k\sigma}^{\mathrm{e}\dagger}d_{\sigma}(\alpha)+d_{\sigma}^{\dagger}(\alpha)c_{k\sigma}^{\mathrm{e}}\right). \tag{3.7}$$

It looks as if the tunneling occurs only between the "even" lead and the nanodisk. Namely, we may neglect the "odd" lead term in the lead Hamiltonian (3.6).

B. Many-Spin Kondo Hamiltonian

The total Hamiltonian is $H=H_{\mathrm{S}}+H_{\mathrm{U}}+H_{\mathrm{L}}+H_{\mathrm{T}}$. We analyze the Hamiltonian $H=H_{0}+H_{\mathrm{T}}$, by taking $H_{0}=H_{\mathrm{U}}+H_{\mathrm{L}}$ as the unperturbed term and H_{T} as the perturbation term. We make a canonical transformation known as the Schrieffer-Wolff transformation[20], $H\rightarrow\widetilde{H}=e^{iG}He^{-iG}$, with G the generator satisfying

$$H_{\mathrm{T}}+\frac{i}{2}\left[G,H_{0}\right]=0. \tag{3.8}$$

We may solve this condition explicitly for the generator,

$$\begin{aligned} G=\frac{1}{Ni}\Bigg[\sum_{\alpha k\sigma}\Bigg\{&\frac{\tilde{t}}{\varepsilon_{\mathrm{d}}-\varepsilon\left(k\right)+U_{\alpha\alpha}^{\prime}}d_{\alpha\sigma}^{\dagger}c_{k\sigma}^{\mathrm{e}\dagger}n_{\alpha\bar{\sigma}}\\ &+\frac{\tilde{t}}{\varepsilon\left(k^{\prime}\right)-\varepsilon_{\mathrm{d}}}d_{\alpha\sigma}^{\dagger}c_{k\sigma}^{\mathrm{e}\dagger}\left(1-n_{\alpha\bar{\sigma}}\right)\Bigg\}\\ &+\sum_{\alpha k\sigma}\sum_{\beta\sigma^{\prime}}\Bigg\{\frac{\tilde{t}}{\varepsilon_{\mathrm{d}}-\varepsilon\left(k\right)+U_{\alpha\beta}^{\prime}}d_{\alpha\sigma}^{\dagger}c_{k\sigma}^{\mathrm{e}\dagger}n_{\beta\sigma^{\prime}}\\ &+\frac{\tilde{t}}{\varepsilon\left(k^{\prime}\right)-\varepsilon_{\mathrm{d}}}d_{\alpha\sigma}^{\dagger}c_{k\sigma}^{\mathrm{e}\dagger}\left(1-n_{\beta\sigma^{\prime}}\right)\Bigg\}-\mathrm{h.c.}\Bigg], \end{aligned} \tag{3.9}$$

where $\bar{\sigma}=\downarrow\uparrow$ for $\sigma=\uparrow\downarrow$, and

$$U_{\alpha\beta}^{\prime}=\left(U_{\alpha\beta}-\frac{J_{\alpha\beta}}{2}\right),\qquad\varepsilon_{\mathrm{d}}=U_{\alpha\alpha}. \tag{3.10}$$

The leading term is the second order term, and given by

$$\begin{aligned} H_{\mathrm{eff}}^{(2)}&=\frac{i}{2}\left[G,H_{\mathrm{T}}\right]\\ &=\frac{-\tilde{t}^{2}}{2N}\sum_{\alpha\beta kk^{\prime}\sigma}\left(\frac{1}{\varepsilon_{\mathrm{d}}-\varepsilon\left(k\right)+U_{\alpha\beta}^{\prime}}+\frac{1}{\varepsilon\left(k^{\prime}\right)-\varepsilon_{\mathrm{d}}}\right)c_{k\sigma}^{\mathrm{e}\dagger}c_{k^{\prime}\sigma}^{\mathrm{e}}\\ &\quad+\frac{2\tilde{t}^{2}}{N}\sum_{\alpha\beta kk^{\prime}\sigma\sigma^{\prime}}\left(\frac{1}{\varepsilon_{\mathrm{d}}-\varepsilon\left(k\right)+U_{\alpha\beta}^{\prime}}-\frac{1}{\varepsilon\left(k^{\prime}\right)-\varepsilon_{\mathrm{d}}}\right)\\ &\qquad\times c_{k\sigma}^{\mathrm{e}\dagger}\boldsymbol{\tau}_{\sigma\sigma^{\prime}}c_{k^{\prime}\sigma^{\prime}}^{\mathrm{e}}\cdot\boldsymbol{S}\left(\alpha\right). \end{aligned} \tag{3.11}$$

The dominant contribution comes from the Fermi surface, $\varepsilon\left(k\right)=\varepsilon_{\mathrm{F}}$. We now assume the SU($N$) symmetry $U_{\alpha\beta}^{\prime}=U^{\prime}$ and the symmetric condition $\varepsilon_{\mathrm{F}}=\varepsilon_{\mathrm{d}}+\frac{U^{\prime}}{2}$ with respect to the Fermi level. Then, the second order term becomes the many-spin Kondo Hamiltonian,

$$H_{\mathrm{K}}\equiv H_{\mathrm{eff}}^{(2)}=J_{\mathrm{K}}\sum_{kk^{\prime}\sigma\sigma^{\prime}}c_{k\sigma}^{\mathrm{e}\dagger}\boldsymbol{\tau}_{\sigma\sigma^{\prime}}c_{k^{\prime}\sigma^{\prime}}^{\mathrm{e}}\cdot\boldsymbol{S}_{\mathrm{tot}}, \tag{3.12}$$

with the Kondo coupling constant

$$J_{\mathrm{K}}=2\tilde{t}^{2}\left(\frac{1}{\varepsilon_{\mathrm{d}}-\varepsilon_{\mathrm{F}}+U^{\prime}}-\frac{1}{\varepsilon_{\mathrm{F}}-\varepsilon_{\mathrm{d}}}\right)=\frac{8\tilde{t}^{2}}{U^{\prime}}. \tag{3.13}$$

The difference between the above many-spin Kondo Hamiltonian and the ordinary Kondo Hamiltonian is whether the local spin is given by the summation over many spins $\boldsymbol{S}_{\mathrm{tot}}$ or a single spin $\boldsymbol{S}$. Note that $\boldsymbol{S}_{\mathrm{tot}}^{2}$ is a dynamical variable but $\boldsymbol{S}^{2}$ is not, $\boldsymbol{S}^{2}=3/4$.

C. Kondo-Heisenberg System

We have derived the Kondo Hamiltonian from the Coulomb and transfer terms by way of the Schrieffer-Wolff transformation. The resultant system is the Kondo-Heisenberg model, which comprises of the Heisenberg Hamiltonian, the lead-electron Hamiltonian and the Kondo Hamiltonian,

$$H_{\text{eff}} = H_{\text{S}} + H_{\text{L}} + H_{\text{K}}, \tag{3.14}$$

where we have ignored H_{U} since it is just a constant at half filling. We note that the order of the Heisenberg Hamiltonian ($\sim U$) is much larger than the order of the Kondo Hamiltonian ($\sim 4\tilde{t}^2/U$) because $U \gg \tilde{t}$.

Our goal is the analysis of the partition function of the coupled system (3.14). We define the spinor $\psi = (c^{\text{e}}_{\uparrow}, c^{\text{e}}_{\downarrow})^t$. The partition function in the Matsubara form is given by

$$Z = \text{Tr}_S \int \mathcal{D}\psi\mathcal{D}\psi^{\dagger} \exp\left[-\int_0^{\beta} d\tau \int dx \, \left(\psi^{\dagger}\partial_{\tau}\psi + \mathcal{H}_{\text{eff}}\right)\right], \tag{3.15}$$

with $\mathcal{H}_{\text{eff}}$ the Hamiltonian density, where the lead electron's degree of freedom is integrated out by a functional integral, and the nanodisk spin is summed up. Since the Heisenberg term does not contain lead electrons, we can separate it as

$$Z = \text{Tr}_S \left[\exp\left(-\beta H_{\text{S}}\right) Z_{\text{K}}\right], \tag{3.16}$$

where $Z_{\text{K}} = \int \mathcal{D}\psi\mathcal{D}\psi^{\dagger} \exp\left[-S_{\text{K}}\right]$, with

$$S_{\text{K}} = \int_0^{\beta} d\tau \int dx \, \left(\psi^{\dagger}\partial_{\tau}\psi + \mathcal{H}_{\text{L}} + \mathcal{H}_{\text{K}}\right). \tag{3.17}$$

First, we evaluate the functional integration Z_{K} in Subsection III D. We obtain the effective spin Hamiltonian, where the only active degree of freedom is the nanodisk spin. Then, we sum up over the nanodisk spin to obtain the total partition function Z. We do this for the graphene lead and for the metallic lead in Subsections III E and III F, respectively.

D. Functional Integration

Because an electron in the lead is constrained within a very narrow region, it is a good approximation to neglect momentum scatterings,

$$H_{\text{K}} \simeq J_{\text{K}} \sum_{k\sigma\sigma'} c^{\text{e}\dagger}_{k\sigma} \boldsymbol{\tau}_{\sigma\sigma'} c^{\text{e}}_{k\sigma'} \cdot \boldsymbol{S}_{\text{tot}}. \tag{3.18}$$

The action (3.17) is summarized as

$$S_{\text{K}} = \int \frac{d\omega}{2\pi} \sum_k \psi^{\dagger}(k) \, M(k) \, \psi(k), \tag{3.19}$$

with

$$M(k) = -[i\omega - \varepsilon(k)] + J_{\text{K}} \boldsymbol{\tau} \cdot \boldsymbol{S}_{\text{tot}}. \tag{3.20}$$

Performing the integration we find

$$Z_{\text{K}} = \text{Det}[M] = \exp\left[-\beta F_{\text{K}}\right], \tag{3.21}$$

where

$$F_{\text{K}} = -\frac{1}{2\beta} \sum_k \ln\left[\cosh \beta J_{\text{K}} \left|\boldsymbol{S}_{\text{tot}}\right| + \cosh \beta\varepsilon(k)\right]. \tag{3.22}$$

is the Helmholtz free energy F_{K}. This formula is reduced to the well-known one for free electrons with the dispersion relation $\varepsilon(k)$ for $J_{\text{K}} = 0$. We evaluate the momentum integral for the graphene lead and for the metallic lead, separately, in the succeeding two subsections.

E. Zigzag Graphene Nanoribbon Leads

We consider the system where the leads are made of zigzag graphene nanoribbons. Owing to the flat band at the zero energy, $\varepsilon(k) = 0$, the result of the functional integration (3.22) is quite simple,

$$F_{\text{K}} = -\frac{1}{\beta} \ln \cosh \frac{\beta}{2} J_{\text{K}} \left|S_{\text{tot}}\right|. \tag{3.23}$$

The effective Hamiltonian for the nanodisk spin is $H_{\text{S}} + F_{\text{K}}$. The lead effect is to make the effective spin stiffness larger and the ferromagnet more rigid.

The partition function (3.16) is

$$Z = \text{Tr}_S \left[\exp\left[\beta J \boldsymbol{S}^2_{\text{tot}}\right] \cosh \frac{\beta}{2} J_{\text{K}} \left|\boldsymbol{S}_{\text{tot}}\right|\right], \tag{3.24}$$

as implies that the eigenstates of the total Hamiltonian are given by $J\boldsymbol{S}^2_{\text{tot}} \pm \frac{1}{2} J_K \left|\boldsymbol{S}_{\text{tot}}\right|$. Namely, the ground states are split into two by the existence of the lead-electron spin. Accordingly, the ground state multiplicity is reduced to $(N+1)/2$, which is just one half of that of the nanodisk without leads.

The trace over the total spin is carried out in (3.24),

$$\begin{aligned} Z = &\sum_{q=0}^{N/2} (N - 2q + 1) \left({}_N C_q - {}_N C_{q-1}\right) \\ &\times \exp\left[\beta J \left(\frac{N}{2} - q\right)\left(\frac{N}{2} - q + 1\right)\right] \\ &\times \cosh\left[\frac{\beta J_{\text{K}}}{2} \sqrt{\left(\frac{N}{2} - q\right)\left(\frac{N}{2} - q + 1\right)}\right]. \end{aligned} \tag{3.25}$$

In Fig.6, we show the specific heat $C_{\text{G}}(T)$, the entropy $S_{\text{G}}(T)$, the magnetization $\left\langle \boldsymbol{S}^2_{\text{tot}} \right\rangle$ and the susceptibility χ for various size N connected with graphene leads.

We compare thermodynamical properties of the nanodisk without leads (Fig.4) and with leads (Fig.6). The significant feature is the appearance of a new peak in the specific heat at $T_{\text{K}} = (J_{\text{K}}/2J)T_c$, though it disappears for large N. We examine the internal energy $E_{\text{G}}(T)$,

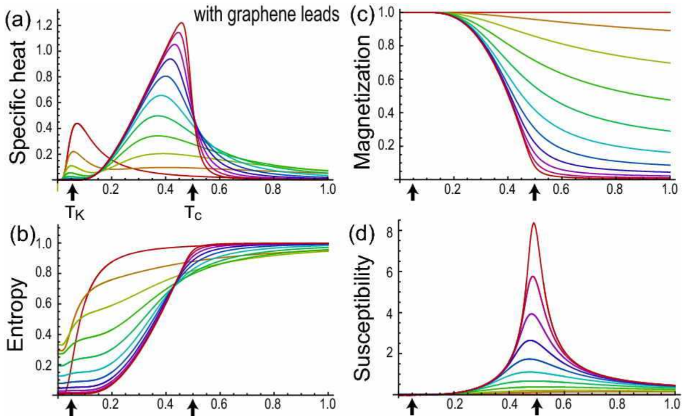

FIG. 6: Thermodynamical properties of the nanodisk-spin system with graphene leads. (a) The specific heat C in unit of $k_{\mathrm{B}}N$. (b) The entropy S in unit of $(k_{\mathrm{B}}N\log 2)$. (c) The magnetization $\langle \boldsymbol{S}_{\mathrm{tot}}^2\rangle$ in unit of S_g^2. (d) The susceptibility χ in unit of S_g. The size is $N=1,2,2^2,\cdots 2^{10}$. We have set $J_{\mathrm{K}}/J=0.2$. The horizontal axis stands for the temperature T in unit of JN/k_{B}. The arrows represents the points corresponding to T_c and T_{K}.

which is found to decrease around T_{K} (Fig.7). Near zero temperature it reads

$$E_{\mathrm{G}}(T)\simeq -JS_g^2-\frac{J_{\mathrm{K}}}{2}S_g+J_{\mathrm{K}}S_g e^{-\beta J_{\mathrm{K}}S_g}. \qquad (3.26)$$

The first term represents the energy stabilization due to the ferromagnetic order present in the nanodisk system without leads, while the second term represents the one due to the Kondo coupling J_{K} between spins in the nanodisk and in the leads. Furthermore, it follows that the entropy is reduced at zero temperature as

$$S_{\mathrm{G}}(0)-S(0)=-k_{\mathrm{B}}\log 2 \qquad (3.27)$$

with (2.19), as implies that the ground state multiplicity at the zero temperature is just one half of that of the system without leads, in accord with the observation made below (3.24). These features indicate the occurrence of the Kondo effect due to the coupling between the spins in the nanodisk and the leads.

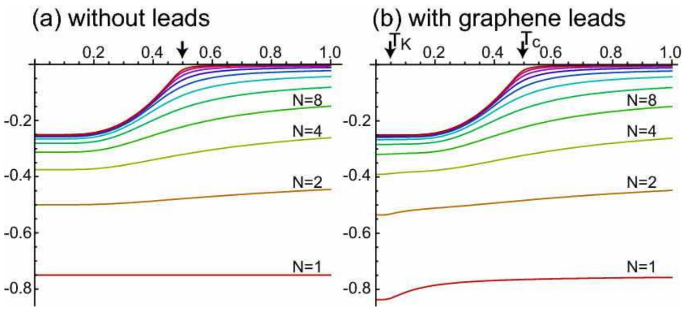

FIG. 7: The internal energy E/Nk_{B} for the system (a) without leads and (b) with graphene leads, for size $N=1,2,4,\cdots 1024$. The horizontal axis stands for the temperature. (a) The energy descreases except for $N=1$ as the temperature decreases, which represents the ferromagnetic order. (b) There exists an additional energy decrease around T_{K}, which is prominent for $N=1$, attributed to the Kondo effect. The arrows represents the points corresponding to T_c and T_{K}.

F. Metallic Leads

Next we consider the system comprised of metallic leads with a constant energy density,

$$\rho(\varepsilon)=\left\{\begin{array}{ll}\rho, & |\varepsilon|<D\\ 0, & |\varepsilon|>D\end{array}\right. . \qquad (3.28)$$

We change the momentum integration into the energy integration in (3.22),

$$F_{\mathrm{K}}=-\frac{\rho}{2\beta}\int_{-D}^{D}d\varepsilon\ln\left[\cosh\beta J_{\mathrm{K}}\left|\boldsymbol{S}_{\mathrm{tot}}\right|+\cosh\beta\varepsilon\right]. \qquad (3.29)$$

The integration is carried out as

$$\begin{aligned}F_{\mathrm{K}}=-\frac{\rho}{\beta}\Big[&\beta DJ_{\mathrm{K}}\left|\boldsymbol{S}_{\mathrm{tot}}\right|-2D\log 2\\&+\frac{1}{\beta}\Big\{\mathrm{Li}_2\big(-e^{\beta(D-J_{\mathrm{K}}|\boldsymbol{S}_{\mathrm{tot}}|)}\big)\\&-\mathrm{Li}_2\big(-e^{-\beta(D+J_{\mathrm{K}}|\boldsymbol{S}_{\mathrm{tot}}|)}\big)\Big\}\Big],\end{aligned} \qquad (3.30)$$

where $\mathrm{Li}_2[x]$ is the dilogarithm function[21],

$$\mathrm{Li}_2[x]=\sum_{n=1}^{\infty}\frac{x^n}{n^2}. \qquad (3.31)$$

It is easy to see that the free energy is reduced to that of the nanodisk-spin system with graphene leads in the limit $D\rightarrow 0$ with $\rho=1/2D$.

In Fig.8, we show the specific heat $C_{\mathrm{M}}(T)$, the entropy $S_{\mathrm{M}}(T)$, the magnetization $\langle \boldsymbol{S}_{\mathrm{tot}}^2\rangle$ and the susceptibility χ for various size N connected with metallic leads.

The behaviors of the magnetization and the susceptibility are the same as those in the case of the nanodisk-spin system with graphene leads. On the other hand, overall behaviors are the same with respect to the specific heat and the entropy. In particular, the same relation as (3.27) holds for the entropy,

$$S_{\mathrm{M}}(0)-S(0)=-k_{\mathrm{B}}\log 2. \qquad (3.32)$$

There are some new features in low temperature regime. Using the asymptotic behaviors[21]

$$\begin{aligned}&\lim_{x\rightarrow\infty}\mathrm{Li}_2[-x]=-\frac{\pi^2}{6}-\frac{1}{2}\log^2\frac{1}{x},\\&\lim_{x\rightarrow 0}\mathrm{Li}_2[-x]=0,\end{aligned} \qquad (3.33)$$

we obtain the free energy, the entropy, the specific heat and the internal energy up to the terms in the order of

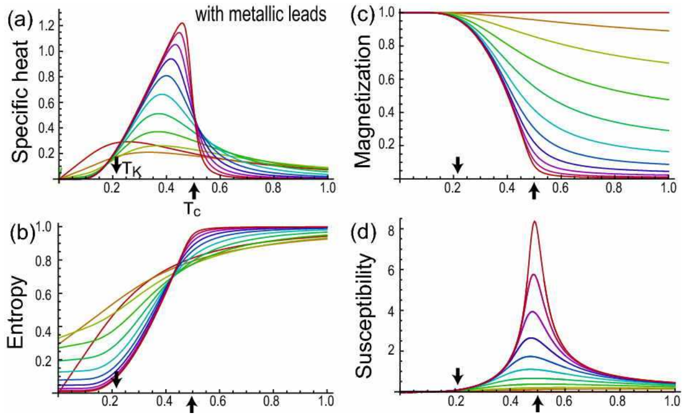

FIG. 8: Thermodynamical properties of the nanodisk-spin system with metallic leads. (a) The specific heat C in unit of $k_{\mathrm{B}}N$. (b) The entropy S in unit of $k_{\mathrm{B}}N\log 2$. (c) The magnetization $\langle \boldsymbol{S}_{\mathrm{tot}}^2 \rangle$ in unit of S_g^2. (d) The susceptibility χ in unit of S_g. The size is $N = 1, 2, 2^2, \cdots 2^{10}$. We have set $J_{\mathrm{K}}/J = 0.2$ and $D = 2k_{\mathrm{B}}T_c$. The horizontal axis stands for the temperature T in unit of JN/k_{B}. The arrows represents the points corresponding to T_c and T_{K}.

$e^{-\beta D}$ as follows,

$$F_{\mathrm{K}} \simeq -\frac{\rho}{\beta}\left[\beta D J_{\mathrm{K}}\left|\boldsymbol{S}_{\mathrm{tot}}\right| - 2D\log 2 + \frac{\pi^2}{6\beta} + \frac{\beta}{2}\left(D - J_{\mathrm{K}}\left|\boldsymbol{S}_{\mathrm{tot}}\right|\right)^2\right], \tag{3.34}$$

$$S_{\mathrm{M}}(T) \simeq k_{\mathrm{B}}\log\frac{N+1}{2} + \frac{\pi^2}{3}\rho k_{\mathrm{B}}^2 T, \tag{3.35}$$

$$C_{\mathrm{M}}(T) \simeq \frac{\pi^2}{3}\rho k_{\mathrm{B}}^2 T, \tag{3.36}$$

and

$$E_{\mathrm{M}}(T) = E_{\mathrm{G}}(T) + \Delta E(T). \tag{3.37}$$

The specific heat $C_{\mathrm{M}}(T)$ is identical to the specific heat of free electrons in the metallic lead. The internal energy $E_{\mathrm{M}}(T)$ consists of two terms: $E_{\mathrm{G}}(T)$ is identical to the energy (3.26) for the nanodisk with graphene leads, and

$$\Delta E(T) \simeq -\frac{\rho}{2}\left(D - J_{\mathrm{K}}S_g\right)^2 + \frac{\pi^2}{6}\rho\left(k_{\mathrm{B}}T\right)^2 \tag{3.38}$$

is the energy for the metallic lead. Here, the first term shows that the band width of free electrons in the lead (3.28) becomes narrower due to the Kondo coupling. We may interpret that n free electrons in the lead with

$$n = \rho J_{\mathrm{K}}S_g \tag{3.39}$$

are consumed to make spin-coupling with electrons in the nanodisk. The second term is the thermal energy of free electrons in the metallic lead.

IV. SPINTRONIC DEVICES AND APPLICATIONS

We propose some applications of graphene nanodisk-lead systems to spintronic devices[22]. The nanodisk-spin system is a quasi-ferromagnet, which is an interpolating system between a single spin and a ferromagnet. It is easy to control a single spin by a tiny current but it does not hold the spin direction for a long time. On the other hand, a ferromagnet is very stable, but it is hard to control the spin direction by a tiny current. A nanodisk quasi-ferromagnet has an intermediate nature: It can be controlled by a relatively tiny current and yet holds the spin direction for quite a long time. Indeed, its life-time τ_{ferro} is given by[12]

$$\tau_{\mathrm{ferro}} \propto \exp\left[\frac{JN^2}{2kT}\right], \tag{4.1}$$

which is quite long compared to the size. The important point is that the size is of the order of nanometer, and it is suitable as a nanodevice.

The coupling of the nanodisk spin and the injected electron spin $\frac{1}{2}\psi^\dagger\boldsymbol{\tau}\psi$ is described by the Landau-Lifschitz-Gelbert equation[22],

$$\frac{\partial \boldsymbol{n}}{\partial t} = \gamma\boldsymbol{B}_{\mathrm{eff}} \times \boldsymbol{n} - \alpha\boldsymbol{n} \times \frac{\partial \boldsymbol{n}}{\partial t}, \tag{4.2}$$

where $\boldsymbol{n} = \boldsymbol{S}_{\mathrm{tot}}/|\boldsymbol{S}_{\mathrm{tot}}|$ is the normalized nanodisk spin, γ is the gyromagnetic ratio, α is the Gilbert damping constant ($\alpha \approx 0.01$), and $\boldsymbol{B}_{\mathrm{eff}}$ is the effective magnetic field produced by the injected electron spin,

$$\boldsymbol{B}_{\mathrm{eff}} = -\frac{U}{\hbar\gamma|\boldsymbol{S}_{\mathrm{tot}}|}\left\langle\psi^\dagger\boldsymbol{\tau}\psi\right\rangle. \tag{4.3}$$

It is proportional to the injected current I^{in}. A spin polarized current rotates the nanodisk spin to the same direction as the current with the relaxation time

$$\tau_{\mathrm{filter}} = \frac{1+\alpha^2}{2\alpha\gamma\left|\boldsymbol{B}_{\mathrm{eff}}\right|} \propto N. \tag{4.4}$$

We use these properties to design spintronic devices.

A. Basic Components of Spintronic Devices

Spin filter: We consider a lead-nanodisk-lead system [Fig.5], where an electron makes a tunnelling from the left lead to the nanodisk and then to the right lead. Lead electrons with the same spin direction as the nanodisk spin can pass through the nanodisk freely. However, those with the opposite direction feel a large Coulomb barrier and are blocked (Pauli blockade)[22]. As a result, when we apply a spin-unpolarized current to the nanodisk, the outgoing current is spin polarized to the direction of the nanodisk spin. Consequently, this system acts as a spin filter.

Spin memory: A nanodisk can be used as a spin memory, where the spin direction is the information. We can read-out the information by applying a spin-unpolarized current because the outgoing current from a nanodisk is spin-polarized to the direction of the nanodisk spin. Furthermore, the direction of the nanodisk spin itself can be controlled by applying a spin-polarized current into the nanodisk.

Spin amplifier: A nanodisk can be used as a spin amplifier. We take the incoming current to be partially polarized, whose average direction is assumed to be up, $I_\uparrow^{\text{in}} > I_\downarrow^{\text{in}} > 0$. On the other hand, the direction of the nanodisk spin is arbitrary. Since spins in the nanodisk feel an effective magnetic field proportional to $I_\uparrow^{\text{in}} - I_\downarrow^{\text{in}}$, they are forced to align with that of the partially-polarized-spin current after making damped precession. After enough time ($\tau \gg \tau_{\text{filter}}$), all spins in the nanodisk take the up direction and hence the outgoing current is the perfectly up-polarized one, $I_\uparrow^{\text{out}} = I_\uparrow^{\text{in}}$, $I_\downarrow^{\text{out}} = 0$. Consequently, the small difference $I_\uparrow^{\text{in}} - I_\downarrow^{\text{in}}$ is amplified to the large current $I_\uparrow^{\text{in}}$. The amplification ratio is given by $I_\uparrow^{\text{in}}/(I_\uparrow^{\text{in}} - I_\downarrow^{\text{in}})$, which can be very large. This effect is very important because the signal of spin will easily suffer from damping by disturbing noise in leads. By amplifying the signal we can make circuits which are strong against noises.

Spin rotator: We can arrange a lead so that it has the Rashba-type interaction[23],

$$H_{\text{R}} = \frac{\lambda}{\hbar}\left(p_x \tau^y - p_y \tau^x\right). \tag{4.5}$$

Spins precess while they pass through the lead. The spin-rotation angle is given[24] by $\theta = 2\lambda m^* L/\hbar$, where m^* is the electron effective mass in the lead and L is the length of the lead. We can control θ by changing the coupling strength λ externally by applying an electric field[25]. In this way we can rotate the direction of spin current by any degree θ. We call such a lead as a spin rotator.

B. Some Spintronic Devices

Spin valve: A nanodisk can be used as a spin valve, inducing the giant magnetoresistance effect[26,27,28]. We set up a system composed of two nanodisks sequentially connected with leads [Fig.9]. We apply external magnetic field, and control the spin direction of the first nanodisk to be $|\theta\rangle = \cos\frac{\theta}{2}|\uparrow\rangle + \sin\frac{\theta}{2}|\downarrow\rangle$, and that of the second nanodisk to be $|0\rangle = |\uparrow\rangle$. We inject an unpolarized-spin current to the first nanodisk. The spin of the lead between the two nanodisks is polarized into the direction of $|\theta\rangle$. Subsequently the current is filtered to the up-spin one by the second nanodisk. The outgoing current from the second nanodisk is $I_\uparrow^{\text{out}} = I\cos\frac{\theta}{2}$. We can control the magnitude of the up-polarized current from 0 to I by rotating the external magnetic field. The system act as a spin valve.

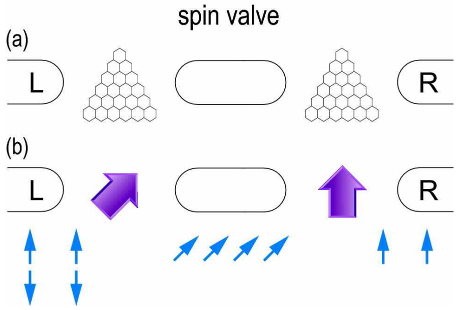

FIG. 9: Illustration of spin valve. (a) The spin valve is made of two nanodisks with the same size, which are connected with leads. (b) Applying external magnetic field, we control the spin direction of the first nanodisk to be $|\theta\rangle$, and that of the second nanodisk to be $|0\rangle = |\uparrow\rangle$. The incomming current is unpolarized, but the outgoing current is polarized, $I_\uparrow^{\text{out}} = I\cos\frac{\theta}{2}$, $I_\downarrow^{\text{out}} = 0$.

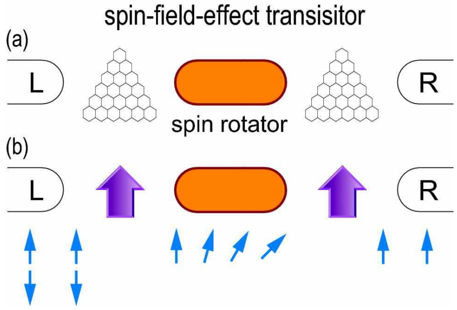

FIG. 10: Illustration of spin-field-effect transistor. (a) It is made of two nanodisks with the same size, which are connected with a rotator. (b) We set the spin direction of the two nanodisks to be up by magnetic field. The incomming current is unpolarized, but the outgoing current is polarized and given by $I_\uparrow^{\text{out}} = I\cos\frac{\theta}{2}$, $I_\downarrow^{\text{out}} = 0$. The up-spin current is rotated by the angle θ within the central lead ascting as a rotator.

Spin-field-effect transistor: We again set up a system composed of two nanodisks sequentially connected with leads [Fig.10]. We now apply the same external magnetic field to both these nanodisks, and fix their spin direction to be up, $|0\rangle = |\uparrow\rangle$. As an additional setting, we use a lead acting as a spin rotator with the spin-rotation angle θ. The outgoing current from the second nanodisk is $I_\uparrow^{\text{out}} = I\cos\frac{\theta}{2}$. It is possible to tune the angle θ by applying an electric field. Hence we can control the magnitude of the up-polarized current. The system acts as a spin-field-effect transistor[29].

Spin diode: We set up a system composed of two nanodisks sequentially connected with leads, where two nanodisks have different sizes [Fig.11]. The left nanodisk is assumed to be larger than the right nanodisk. Then the relaxation time of the left nanodisk $\tau_{\text{filter}}^{\text{L}}$ is larger than that of the right nanodisk $\tau_{\text{filter}}^{\text{R}}$, $\tau_{\text{filter}}^{\text{L}} > \tau_{\text{filter}}^{\text{R}}$. Second, we apply the same magnetic field to the two nanodisks, but we take it so small that the nanodisk spin can be

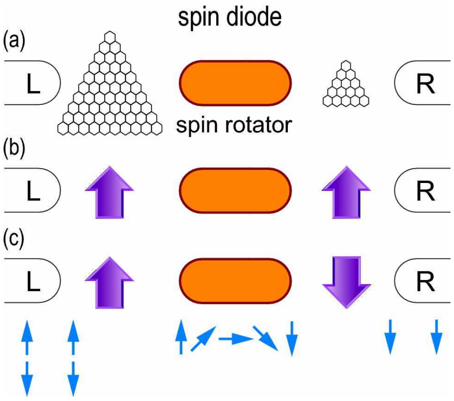

FIG. 11: Illustration of spin diode. (a) It is made of two nanodisks with different size, which are connected with a rotator. (b) We set initially the spin direction of the two nanodisks to be up by weak magnetic field. By controlling the bias voltage, the current flows from the left lead to the right lead, or in the opposite way. (c) We inject an unplolarized current from left (right), which is made up-polarized by the left (right) nanodisk, and then rotated by the central lead. The spin of the right (left) nanodisk is rotated after the relaxation time $\tau_{\text{filter}}^{\text{R}}$ ($\tau_{\text{filter}}^{\text{L}}$). When the incoming current is an unpolarized pulse, the charge transported by the current is different whether it is injected from left or right. This acts as a spin diode.

controlled by a polarized current. For definiteness we take the direction of the magnetic field to be up. Third, the central lead is taken to be a spin rotator with $\theta \approx \pi$. When no currents enter the nanodisk, the directions of the two nanodisk spins are identical due to the tiny external magnetic field, which is up. This is the "off" state of the spin diode. When we inject an unpolarized current to this system, the outgoing current is initially very small, $I^{\text{out}} = I \cos\theta \simeq 0$ for $\Delta\theta \approx \pi$. However, after the relaxation time τ_{filter}, the outgoing current becomes large since the polarized current rotates the spin of the second nanodisk by the angle θ. It takes a longer time when the nanodisk size is larger. Now, let us inject an unpolarized pulse current either from left or from right. It follows that $Q^{\text{L}\to\text{R}} > Q^{\text{R}\to\text{L}}$ since $\tau_{\text{filter}}^{\text{L}} > \tau_{\text{filter}}^{\text{R}}$, where $Q^{\text{L}\to\text{R}}$ and $Q^{\text{R}\to\text{L}}$ are the charges transported by the current injected to the right and left leads, respectively. Hence the system acts as a spin diode.

C. Spin Logic Gates

We can construct spin logic gates in which the spin direction takes logic values; truth (false) identified with up (down) spin, by controlling a spin current by another spin current according to the following setups.

Spin inverter (spin NOT gate): We take a spin rotator with the rotation angle $\theta = \pi$. This rotator is used as a spin NOT gate, by regarding up spin as "true" and down spin as "false", because it interchanges up spin with down spin.

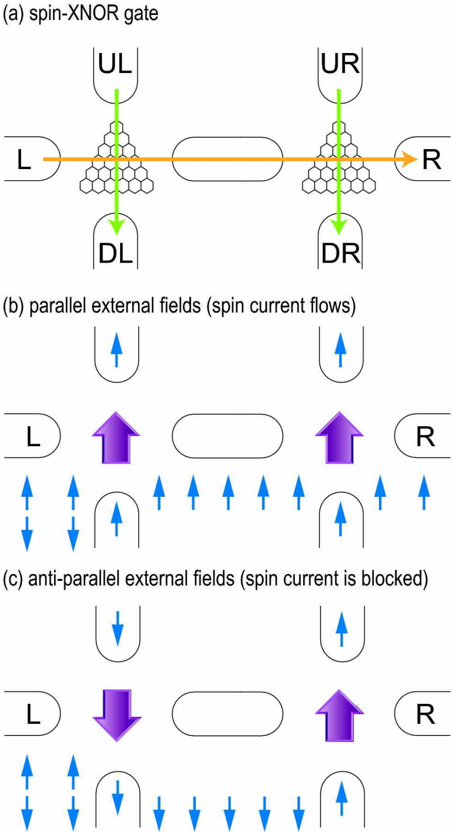
(a) spin-XNOR gate
UL
UR
L
R
DL
DR
(b) parallel external fields (spin current flows)
L
R
(c) anti-parallel external fields (spin current is blocked)
L
R

FIG. 12: (a) Illustration of spin-XNOR gate with unpolarized current coming from left. The unpolarized current is filtered by the left nanodisk, and only up-spin electrons go through the centeral lead. (b) When we apply vertical spin currents with parallel spin direction, the out going current exist. (c) When we apply vertical spin currents with antiparallel spin direction, the out going current does not exist.

Spin XNOR: We may construct a spin XNOR gate. We set up a system composed of two nanodisks connected with seven leads, three horizontal leads and four vertical leads, as illustrated in Fig. 12. We control the nanodisk spins by vertically applied spin currents instead of external magnetic field. We inject an unpolarized current from the left lead to the right lead. When the spin directions of the two vertical spin currents are parallel, the directions of the two nanodisk spins become parallel, and the horizontal current can pass through. However, when the spin directions of the two vertical spin currents are antiparallel, the horizontal current cannot pass through. This system act as a spin XNOR gate by regarding up spin as "true" and down spin as "false".

Spin XOR: We may construct a spin XOR gate by changing the central lead to be a spin rotator with the rotation angle $\Delta\theta = \pi$. The horizontal current passes through if the spin directions of the two vertical spin currents are antiparallel and cannot pass through if they are parallel, as illustrated in Fig. 13.

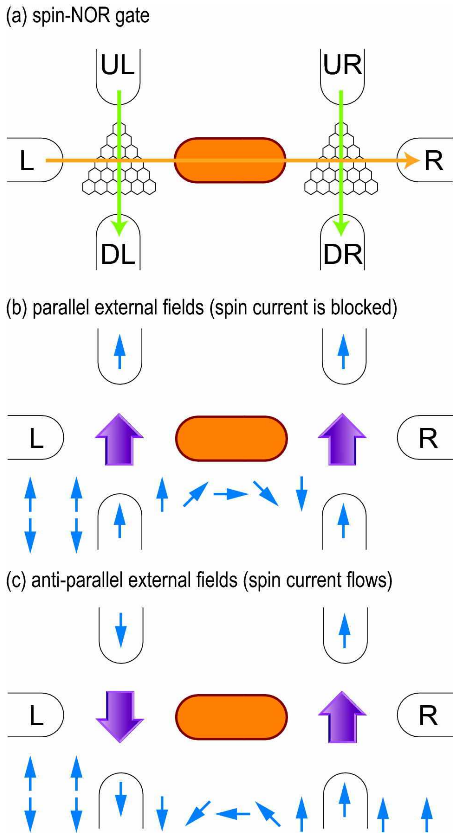
(a) spin-NOR gate
UL
UR
L
R
DL
DR
(b) parallel external fields (spin current is blocked)
L
R
(c) anti-parallel external fields (spin current flows)
L
R

FIG. 13: (a) Illustration of spin-XOR gate with unpolarized current coming from left. The unpolarized current is filtered by the left nanodisk, and only up-spin electrons go through the centeral lead. The electron spin in the central lead rotates $\theta = \pi$ by the Rashba-type interaction. (b) When we apply vertical spin currents with parallel spin direction, the out going current does not exist. (c) When we apply vertical spin currents with antiparallel spin direction, the out going current exist.

V. CONCLUSIONS

The trigonal zigzag nanodisk has a remarkable property that it has N-fold degenerate zero-energy states with the SU(N) symmetry when its size is N. The SU(N) symmetry is broken but not so strongly by the Coulomb interactions. The system is well approximated by the infinite-range Heisenberg model, where the site index runs over these N-fold degenerate states. We may regard it as a quasi-ferromagnet characterized by the exchange energy as large as the Coulomb energy. The relaxation time is finite but quite large even if the size is very small.

In this paper we have investigated thermodynamical properties of a nanodisk. We have found the emergence of a quasi-phase transition between the quasi-ferromagnet and the quasi-paramagnet as a function of temperature even for samples with $N \approx 100$. The transition point T_c is signaled by a sharp peak in the specific heat and in the susceptibility.

We have also examined how they are modified when the external leads are attached to the nanodisk. The lead effects are summarized by the many-spin Kondo Hamiltonian. One effect is to enhance the ferromagnetic order. This result is important to make spintronic circuits by connecting leads in nanodevices. It is also prominent that a new peak appears in the specific heat but not in the susceptibility for small N. The peak position is $T_{\text{K}} = (J_{\text{K}}/2J)T_c$ for the zigzag graphene nanoribbon lead. The energy is found to decrease around the peak position, and the entropy is lowered by factor $k_{\text{B}} \log 2$ in the zero-temperature limit, indicating the Kondo effect due to a Kondo interaction between electrons in the lead and the nanodisk.

We have proposed some applications of nanodisks to nanodevices. Being a ferromagnet, it can be used as a spin filter. Namely, only electrons with spin parallel to the spin of the nanodisk can pass through it. Additionally, it has a novel feature that it is not a rigid ferromagnet. The incoming spin-polarized current can rotate the nanodisk spin itself. Combining the advantages of both these properties, we have proposed a rich variety of spintronic devices, such as spin memory, spin amplifier, spin diode, spin valve and spin-field-effect transistor. Furthermore, we have proposed some spin logic gates such as spin XNOR gate and XOR gate. Graphene nanodisks could well be basic components of future nanoelectronic and spintronic devices.

I am very much grateful to N. Nagaosa for many fruitful discussions on the subject. This work was supported in part by Grants-in-Aid for Scientific Research from the Ministry of Education, Science, Sports and Culture No. 20840011.

---

[1] K. S. Novoselov, A. K. Geim, S. V. Morozov, D. Jiang, Y. Zhang, S. V. Dubonos, I. V. Grigorieva, and A. A. Firsov, Science **306**, 666 (2004).
[2] K. S. Novoselov, A. K. Geim, S. V. Morozov, D. Jiang, M. I. Katsnelson, I. V. Grigorieva, S. V. Dubonos, and A. A. Firsov, Nature **438**, 197 (2005).
[3] Y. Zhang, Y. -W Tan, H. L. Stormer, and P. Kim, Nature **438**, 201 (2005).
[4] M. Fujita, K. Wakabayashi, K. Nakada, and K. Kusakabe, J. Phys. Soc. Jpn. **65**, 1920 (1996).
[5] M. Ezawa, Phys. Rev. B, **73**, 045432 (2006).
[6] L. Brey, and H. A. Fertig, Phys. Rev. B, **73**, 235411 (2006).
[7] F. Muñoz-Rojas, D. Jacob, J. Fernández-Rossier, and J. J. Palacios, Phys. Rev. B, **74**, 195417 (2006).
[8] Y. -W Son, M. L. Cohen, and S. G. Louie, Phys. Rev. Lett., **97**, 216803 (2006).
[9] V. Barone, O. Hod, and G. E. Scuseria, Nano Lett., **6**, 2748 (2006).
[10] M. Y. Han, B. Oezyilmaz, Y. Zhang, and P. Kim, Phys. Rev. Lett., **98**, 206805 (2007).

[11] M. Ezawa, Physica Status Solidi (c) **4**, No.2, 489 (2007).
[12] M. Ezawa, Phys. Rev. B **76**, 245415 (2007): M. Ezawa, Physica E **40**, 1421-1423 (2008).
[13] J. Fernández-Rossier, and J. J. Palacios, Phys. Rev. Lett. **99**, 177204 (2007).
[14] O. Hod, V. Barone, and G. E. Scuseria, Phys. Rev. B **77**, 035411 (2008).
[15] M. Ezawa, Phys. Rev. B **77**, 155411 (2008).
[16] W. L. Wang, S. Meng and E. Kaxiras, Nano Letters **8**, 241 (2008).
[17] W. L. Wang, O. V. Yazyev, S. Meng, and E. Kaxiras, Phys. Rev. Lett. **102**, 157201 (2009).
[18] H. J. Räder, A. Rouhanipour, A. M. Talarico, V. Palermo, P. Samorì, and K. Müllen, Nature materials **5**, 276 (2006).
[19] W. G. van der Wiel, S. De Franceschi, J. M. Elzerman, T. Fujisawa, S. Tarucha and L. P. Kouwenhoven, Rev. Mod. Phys. **75**, 1 (2003).
[20] J. R. Schrieffer and P. A. Wolff, Phys. Rev. **149,** 491 (1966).
[21] M. Abramowitz and I. A. Stegun, Handbook of Mathematical Functions with Formulas, Graphs, and Mathematical Tables, New York: Dover, 1004-1005, (1972).
[22] M. Ezawa, Eur. Phys. J. B **67**, 543 (2009)
[23] E. I. Rashba, Fiz. Tverd. Tela (Leningrad) **2**, 1224 (1960) [Sov. Phys. Solid State **2**, 1109 (1960)]; Y. A. Bychkov and E. I. Rashba, J. Phys. C **17**, 6039 (1984).
[24] I. Zǔtić, J. Fabian and S. Das Sarma, Rev. Mod. Phys., **76**, (2004), and references therin.
[25] J. Nitta, T. Akazaki, and H. Takayanagi, Phys. Rev. Lett. **78**, 1335 (1997).
[26] M. N. Baibich, J. M. Brot, A. Fert, N. V. Dau and F. Petroff, Phys. Rev. Lett. **61**, 2472 (1988).
[27] G. Binasch, P. Grunberg, F. Saurenbach and W. Zinn, Phys. Rev. B **39**, 4828 (1989).
[28] Y. M. Lee, J. Hayakawa, S. Ikeda, F. Matsukura and H. Ohno, Appl. Phys. Lett. **90**, 212507 (2007).
[29] S. Datta and B. Das, Appl. Phys. Lett. **56**, 665 (1990).